Heat transfer, cryostat, (conduction-)cooling (II of II)

CAS – Austria 2023

R. van Weelderen (CERN)

With contributions from P. Borges de Sousa (CERN), T. Kottig (CERN), F. Ferrand (CERN)

Outline

- Fully immersed in HeII:
  - LHC dipoles and HL-LHC cable-stacks
  - Bayonet HX cooling scheme
  - Numerical tool & application to HL-LHC Nb_3Sn quadrupoles
- Helium availability and typical LHC reliance (fully immersed magnets)
- Food for thought of operating fully helium immersed accelerator magnets
- Some points to remember
- References

Fully immersed in HeII: LHC-dipoles

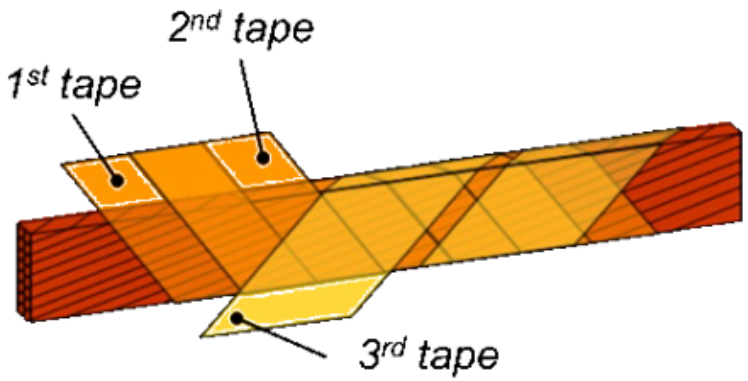

NbTi - cable is:

- non-impregnated

- Electrically insulated by partially overlapping layers of Kapton

--> porous to helium

Fully immersed in HeII: LHC-dipoles

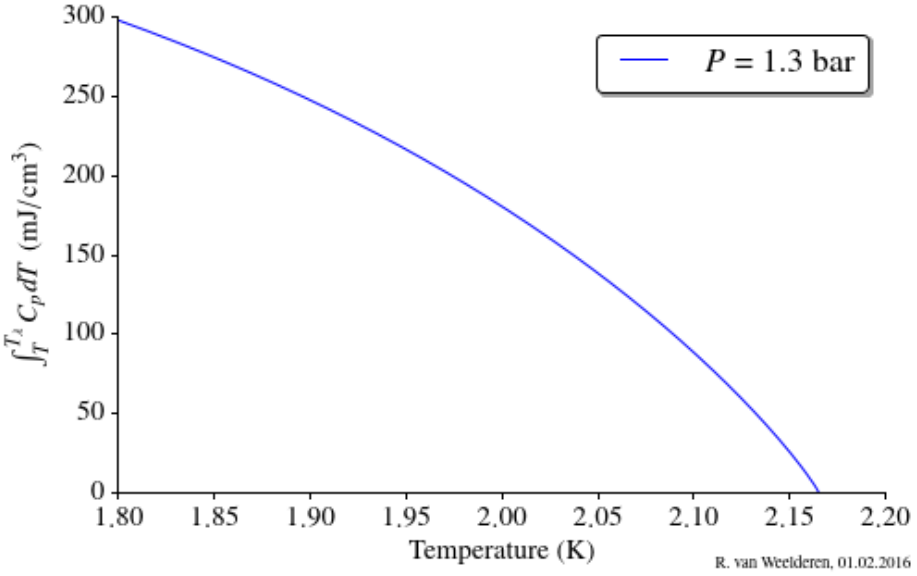

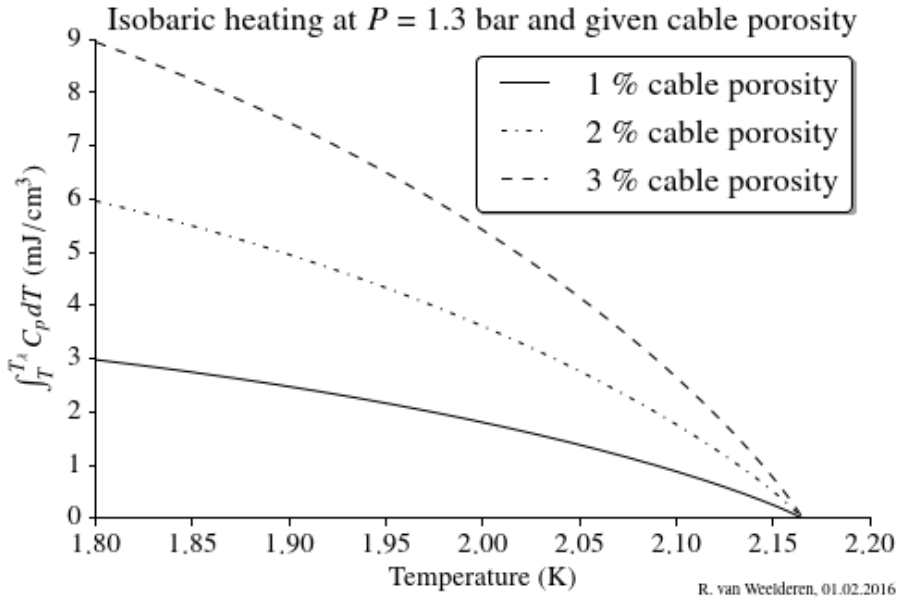

The high thermal capacity of the helium inside the porous NbTi - cable contributes to the stability

The order of magnitude is ~2 mJ/cm³ per % of He volume

Cold-source Heat sources and heat-sinks

(aka “cold-sources”)

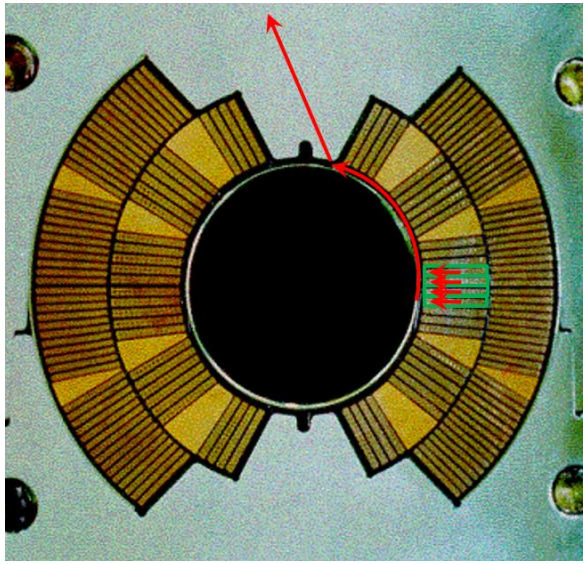

In *fully immersed* magnets the heat generated in the coil-pack must find its way out to the cold-source via helium path-ways kept clear in the cold-mass construct

In the example top left, of the LHC main dipole, heat flows from the coil pack into the annular space between beam-pipe and coil-pack and out via space between the collar laminations

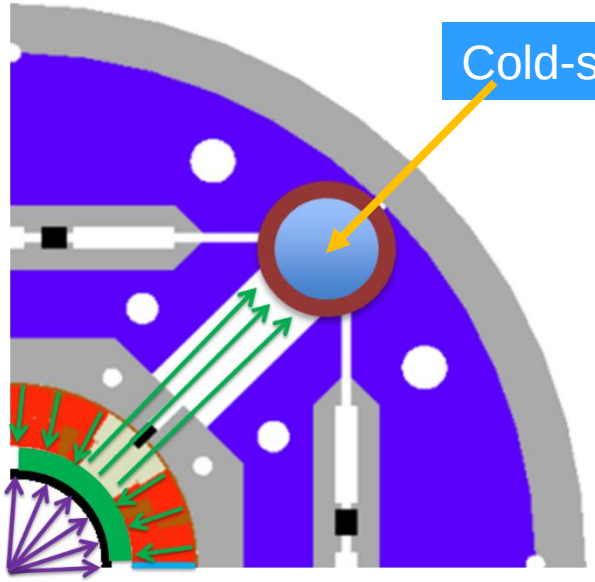

In the example bottom left, of the HL-LHC MQXF quadrupole, heat flows from the coil pack into the annular space between beam-pipe and coil- pack and out via dedicated passages (8 mm diameter holes every 50 mm along the length of the magnet)

Heat sources and heat-sinks

(aka “cold-sources”)

In a *“dry”* magnets the heat generated in the coil-pack must find its way out to the cold-source via solid conduction and solid-liquid interface

Mechanical Concept CERN, CNAO, INFN and MedAUSTRON on novel ion gantry concepts: “dry” conduction cooled magnet

1. Epoxy-impregnated 2-layer coils with inter-layer splice, wound with 34-strand 8.75 mm Nb-Ti cable with braided glass insulation

2. Stiff austenitic steel collars with 0.15..0.2 mm thick spacers on one side to follow the coil curvature

3. Horizontally split laminated iron yoke made of 1-mm-thick Si-steel with b-staged resin coating. Yoke sectors machined out of cured lamination stacks.

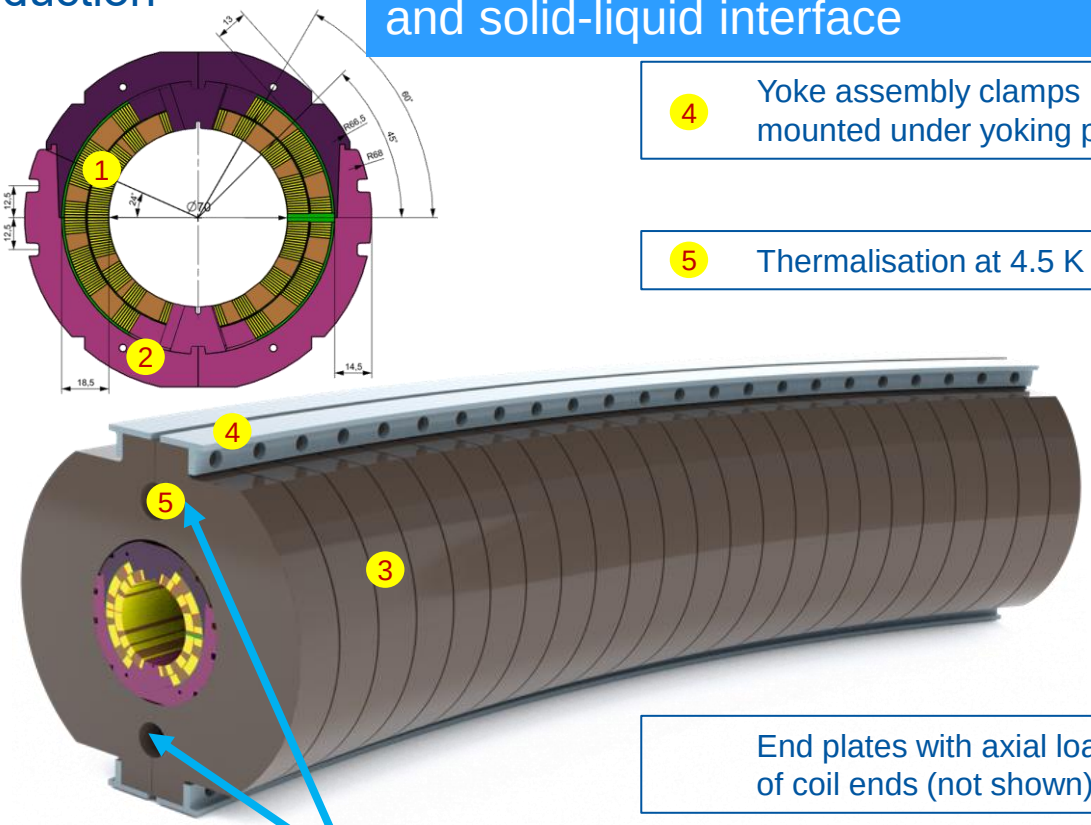

4. Yoke assembly clamps mounted under yoking press

5. Thermalisation at 4.5 K

End plates with axial loading of coil ends (not shown)

Courtesy M. Karpinnen & Ch. Kokkinos

Fully immersed in HeII

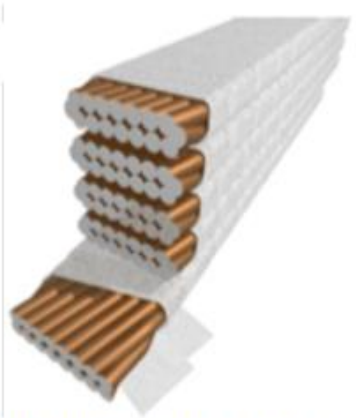

Cable T excursions w.r.t. helium bath measured as function of power deposit

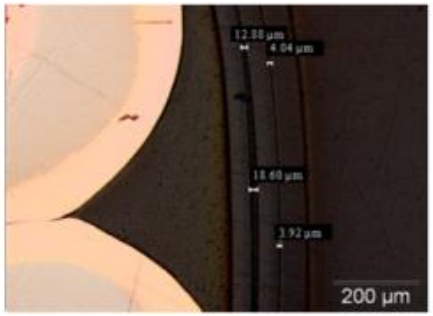

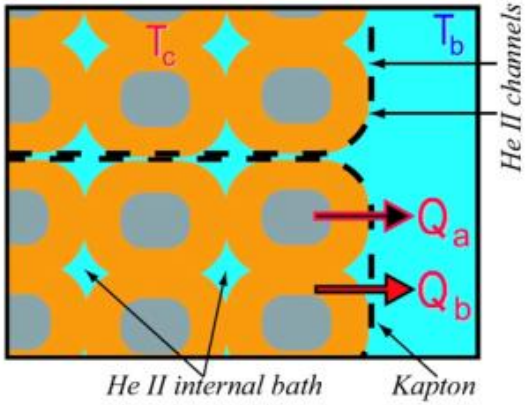

NbTi cables showing the porosity w.r.t. helium

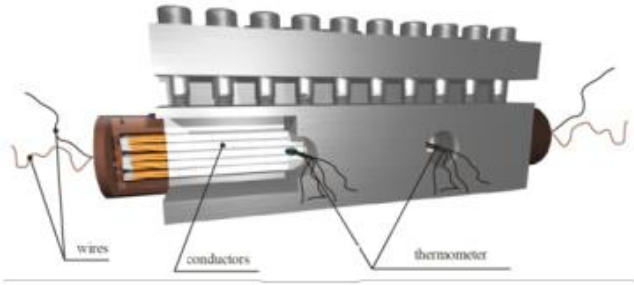

courtesy H. R. Correia Rodrigues

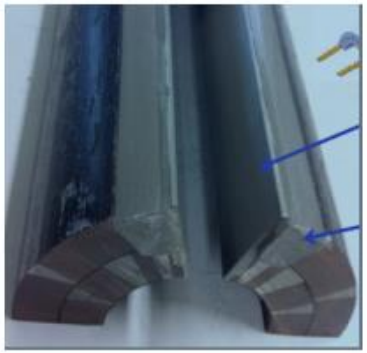

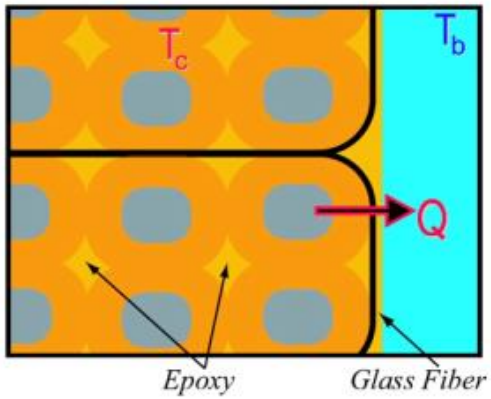

Nb3Sn cables, fully impregnated, only conduction through solids

Fully immersed in HeII

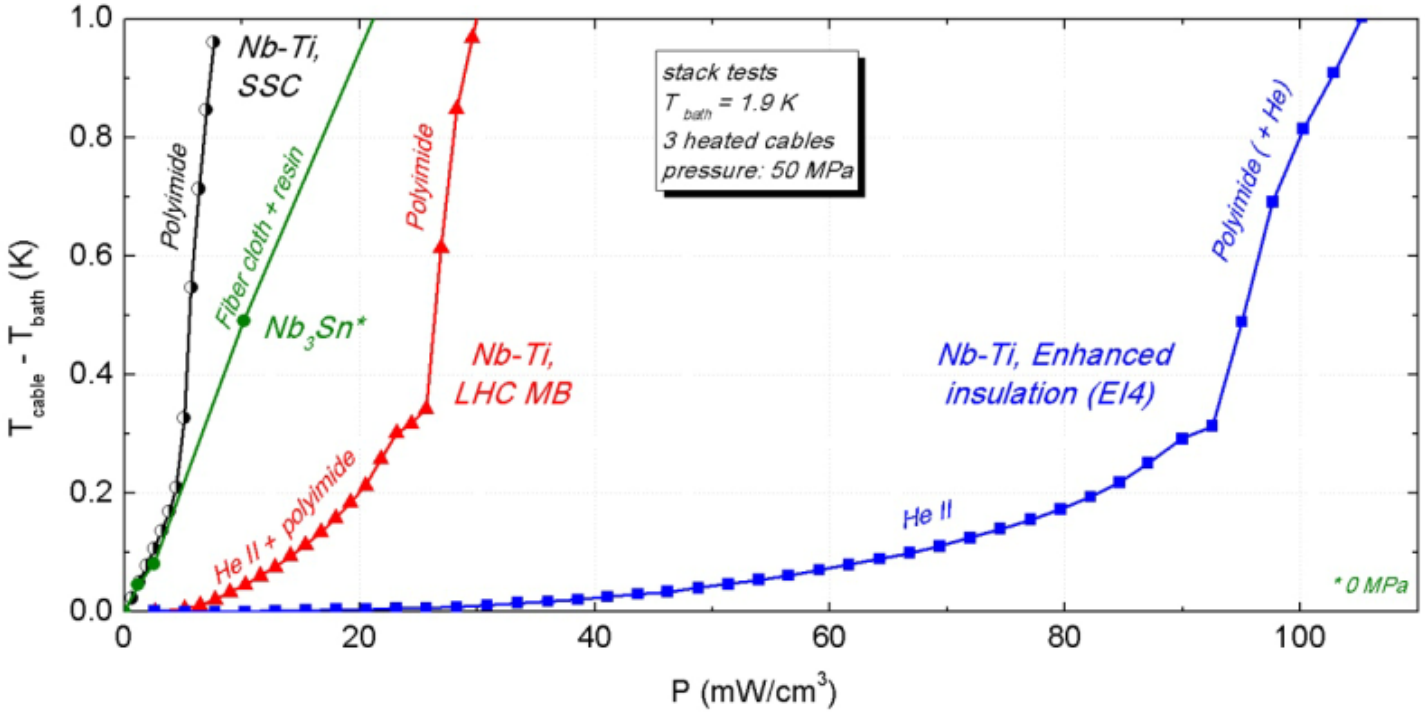

Stack measurement results, all faces open, showing the stark difference between porous and fully impregnated cables

Nb_3Sn measurements have since, the last 5 years, been addressed in more detail (see [3])

Fully immersed in HeII: LHC-dipoles

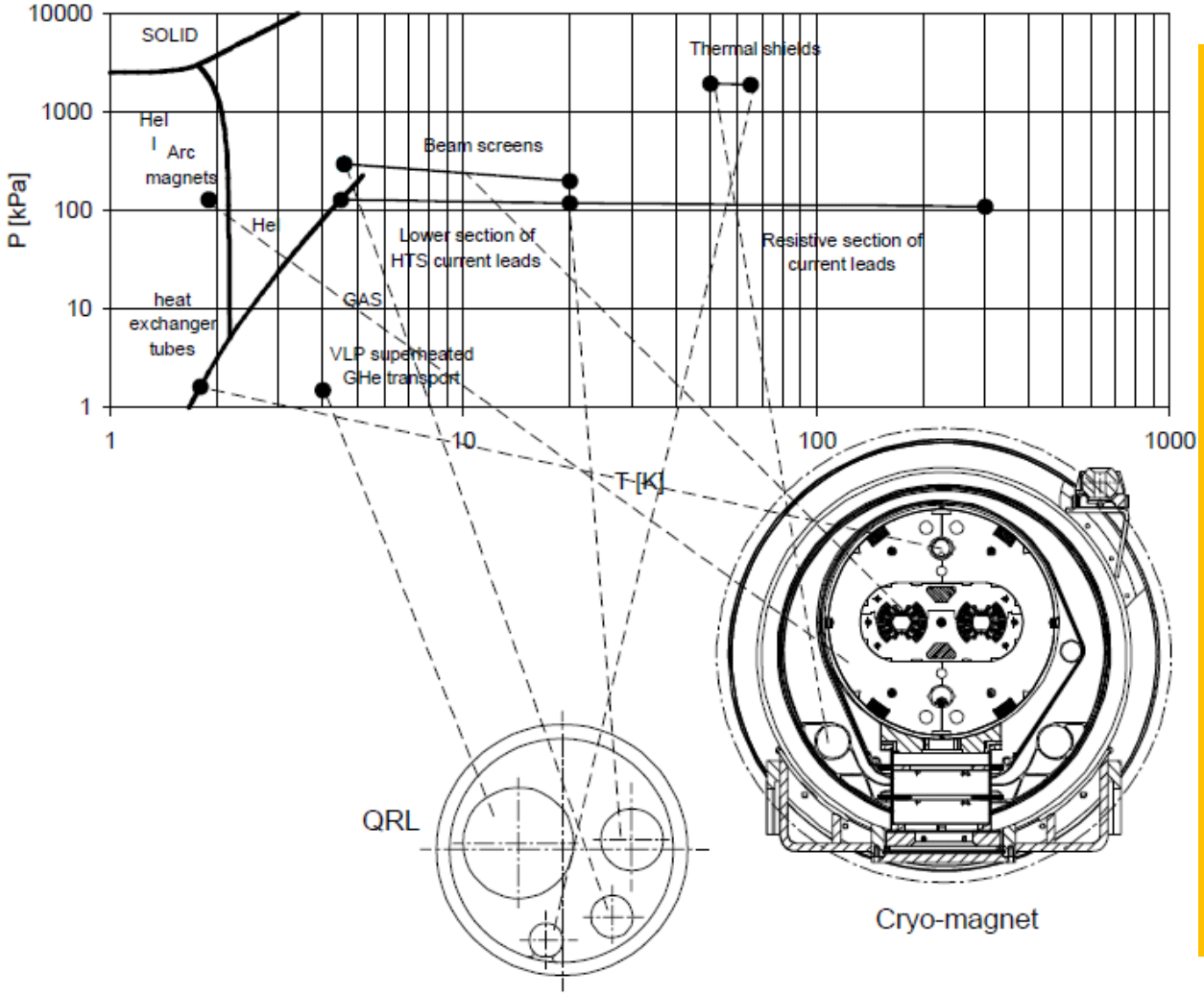

Addressing yesterday's question:

Even if the coil, collar and yoke are in pressurized HeII at 1.3 bar and ~ 1.9 K

The heat-sink (upper hole), where the heat is taken up by vapourizing liquid helium (~1.85 K, ~15 mbar) is in a copper-pipe protruding over the length of several magnets (107 m)

Fully immersed in HeII: LHC-dipoles

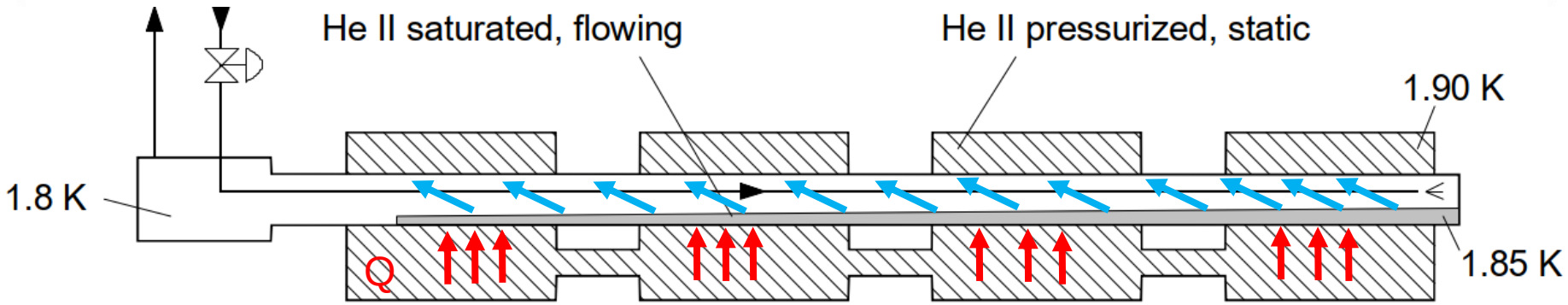

All the extracted heat has eventually to flow across the tube wall, where it encounters three thermal impedances in series:

- the limited solid conduction across the metal constitutive of the wall,
- the Kapitza resistances produced by the refraction of thermal phonons at the metal-to-helium interfaces.

The overall transverse impedance was measured on fully wetted test samples at varying temperature, so that the different temperature dependence of the solid conduction and Kapitza terms enabled to resolve them. For tubes with a wall thickness up to about 1 mm, the Kapitza resistance largely dominates below 2 K, and the use of high-purity, cryogenic-grade copper is not required.

See ref[1, 2]

Evaporation of two-phase, very low pressure, helium flow

Fully immersed in HeII: MQXF

(HL-LHC Nb_3Sn quadrupoles)

- In the context of HL-LHC at CERN, **a robust multi-region CFD numerical framework** for the modelling of **heat transfer in complex cryogenic system geometries involving He II** has been developed
- Numerical tool allowed to **provide thermal design requirements early enough in the magnets' design phase**
- Now, **a fully upgraded and consolidated tool** is used to reassess previous results, and for systematic analysis of heat extraction pathways in complex He II – composite solid geometries

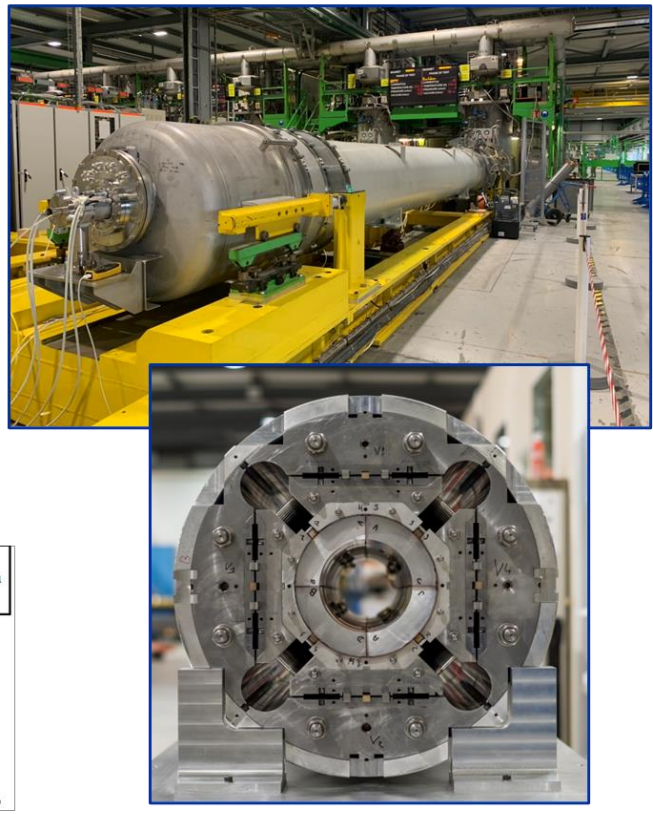

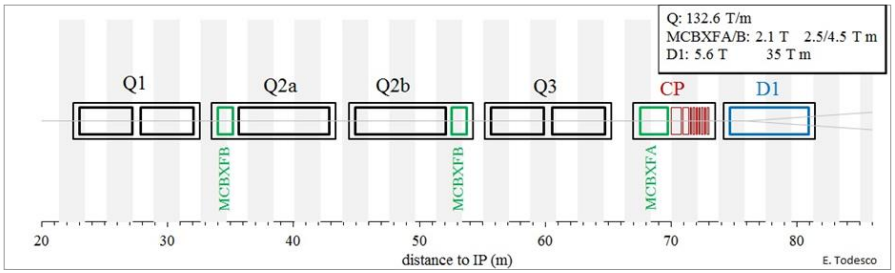

Following slides: courtesy P. Borges de Sousa | Revised estimates of temperature margins in MQXF, see also ref[x]

Numerical code applied to full-scale cold masses

- **Libraries and solver** implemented in OpenFOAM v7, **geometry** created via Python API for Salome, easily adjustable for **parametric studies**
- Currently handles **2D geometries** and **static He II conditions** (no flow) and **He II → He I transition**
- **Power deposition data** can be mapped directly onto the geometry, or **direct heat input** to any part
- **Coil described in detail;** mesh composed of 3.5M cells, **special refinement on thin layers**

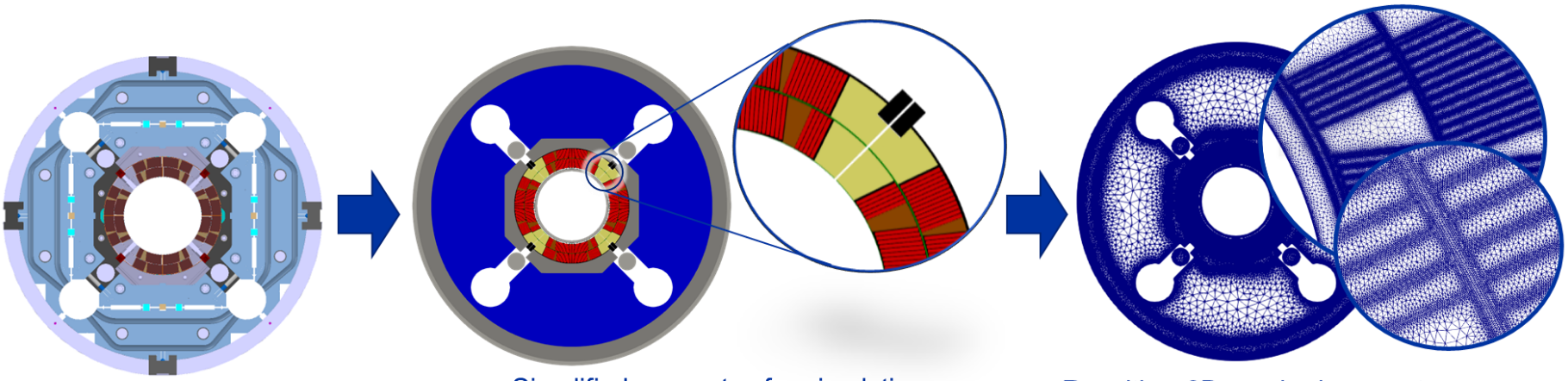

MQXF v7 + cold mass (ST0703448)

Simplified geometry for simulation (coded in Python and Salome)

Resulting 2D meshed geometry (coded in Python and Salome)

MQXF cold mass geometry – composite solid

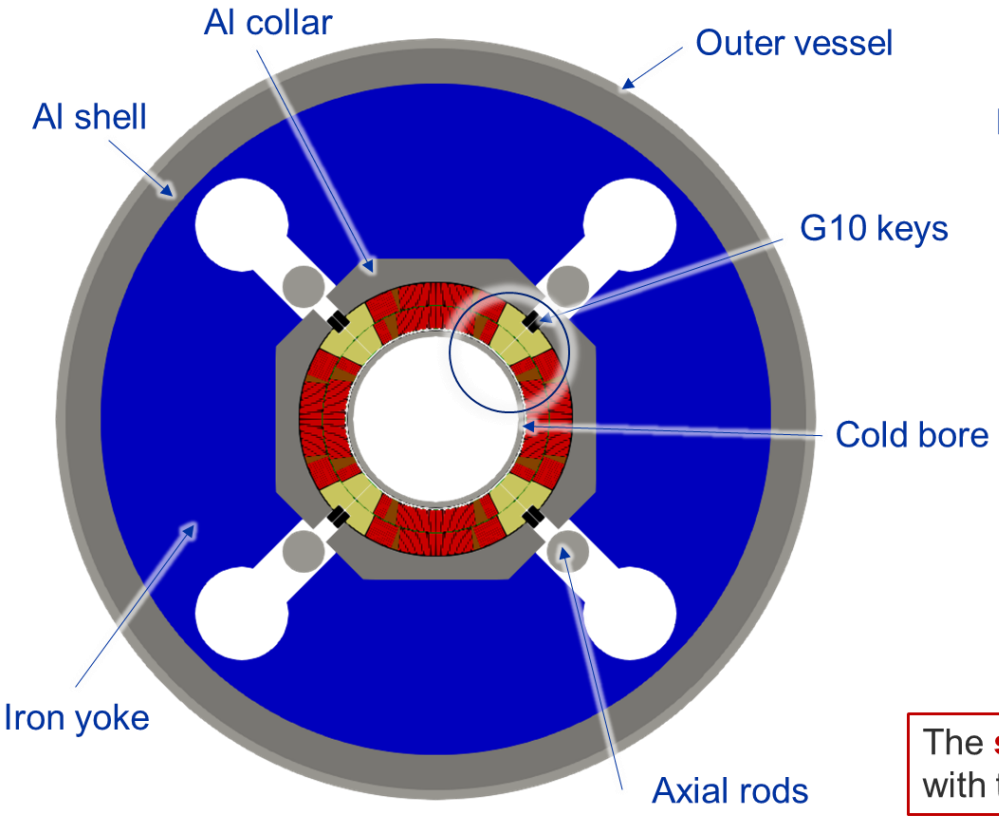

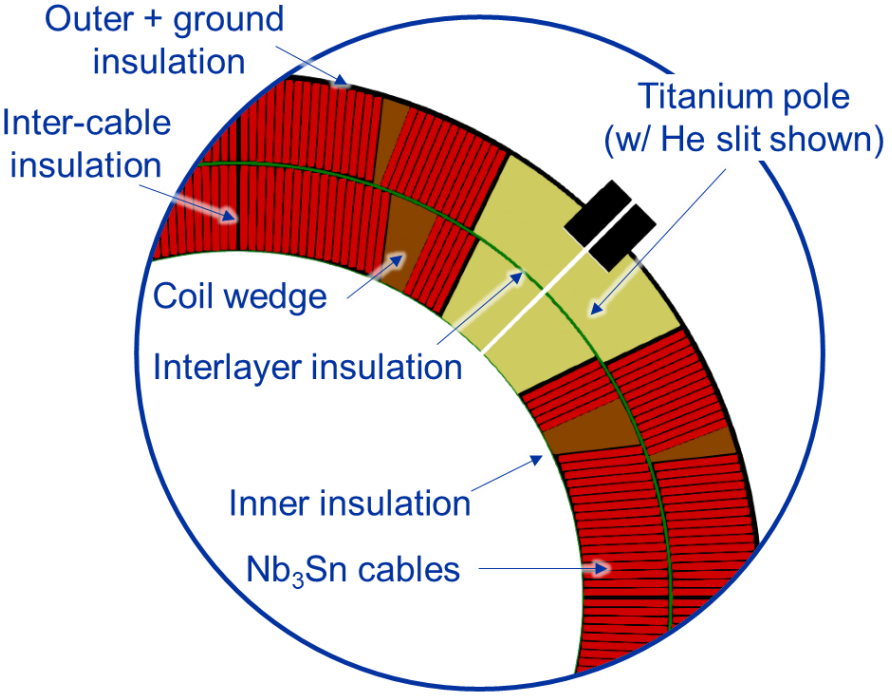

The **solid region** is composed of 17 different zones, each with their own temperature-dependent material properties

MQXF cold mass geometry – He II region

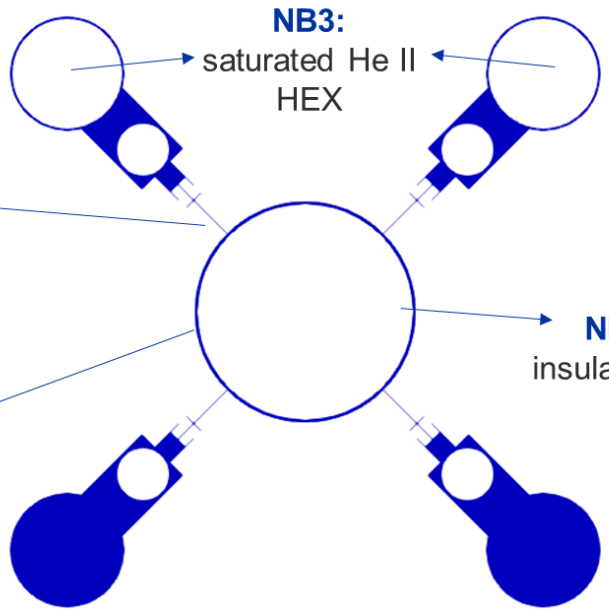

The **He II region** is modelled as a static pressurised bath in contact with the saturated He II heat exchangers at a constant temperature

The connection between annular space and HEX passages is modelled as a continuous 1 mm slit over the cold mass' length

Input for heat deposition from dose calculations (I)

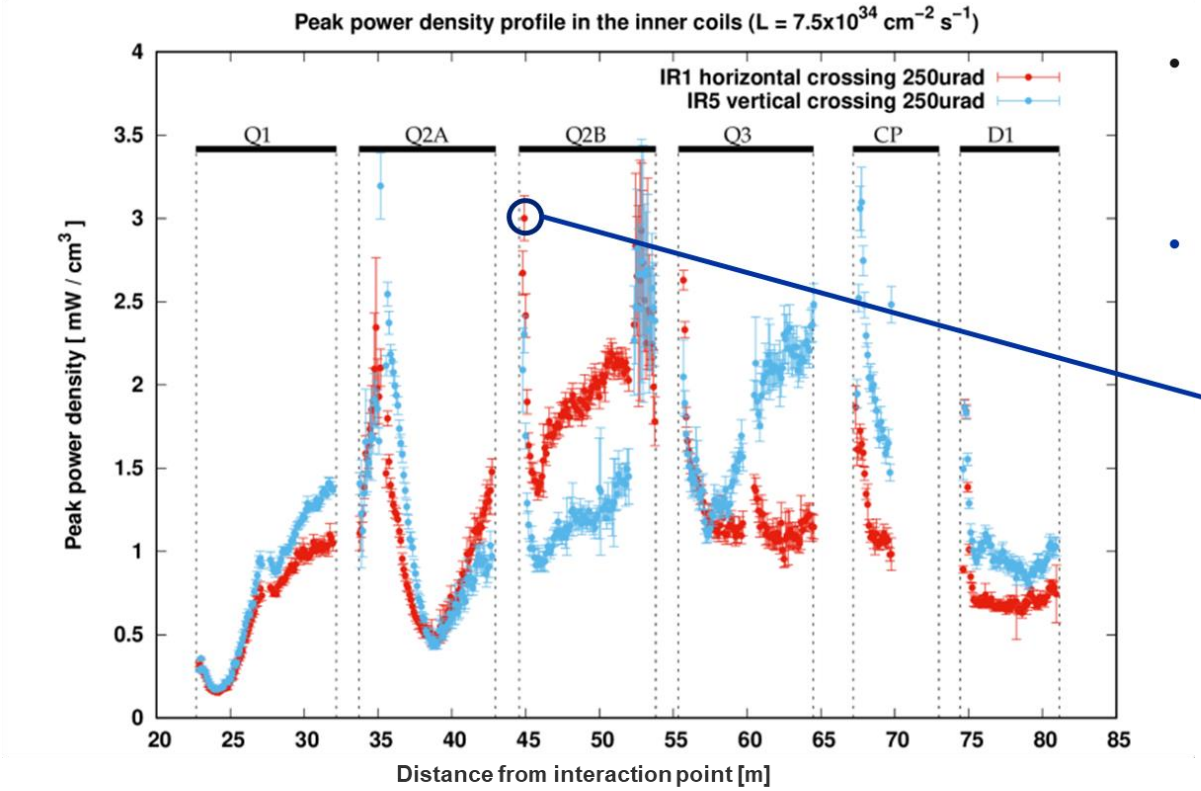

- For each magnet/cold mass, **the cross-section that corresponds to the highest dose** (and consequently heat load) is selected
- **12 cross-sections selected** (Q1/2/3 A and B, vertical and horizontal crossings)

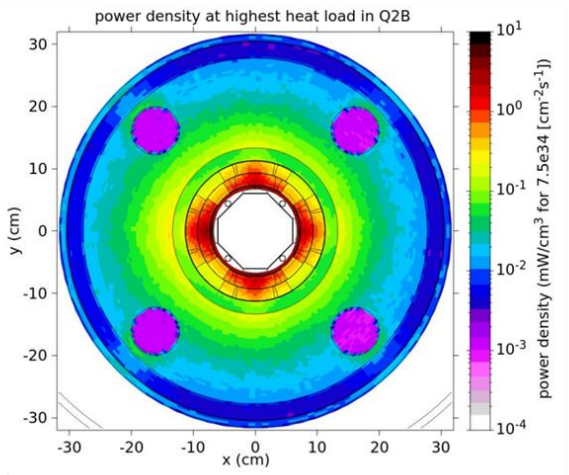

Source: Review of estimates of energy deposition, M. Sabate-Gilarte

Input for heat deposition from dose calculations (II)

- For each cold mass, the 2D **power density** (mW/cm^3) **at the peak** (maximum) **location** for nominal luminosity (7 TeV, 5.0x10^{34} cm^{-2}s^{-1}) is mapped onto the mesh
- Mesh is split into two regions, a **He II region** and a **solid region**
- Set of **boundary conditions** is chosen; power density map changes for every analysed cross-section

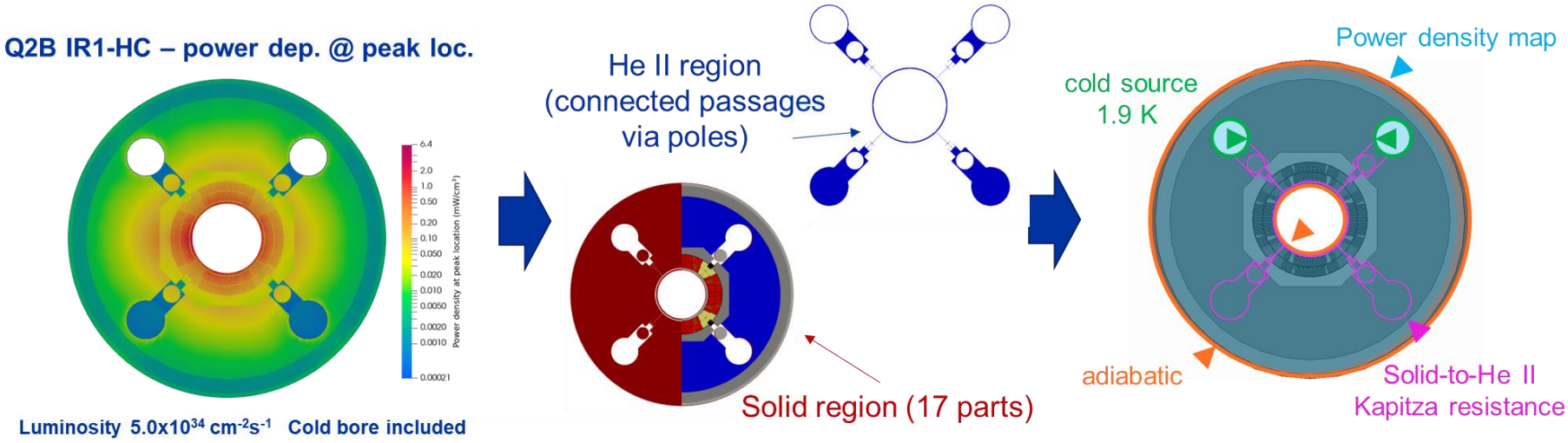

Results: example Q2B IR1-HC @ nominal luminosity

Temperature distribution at peak location

Temp. distribution at peak location (coil detail)

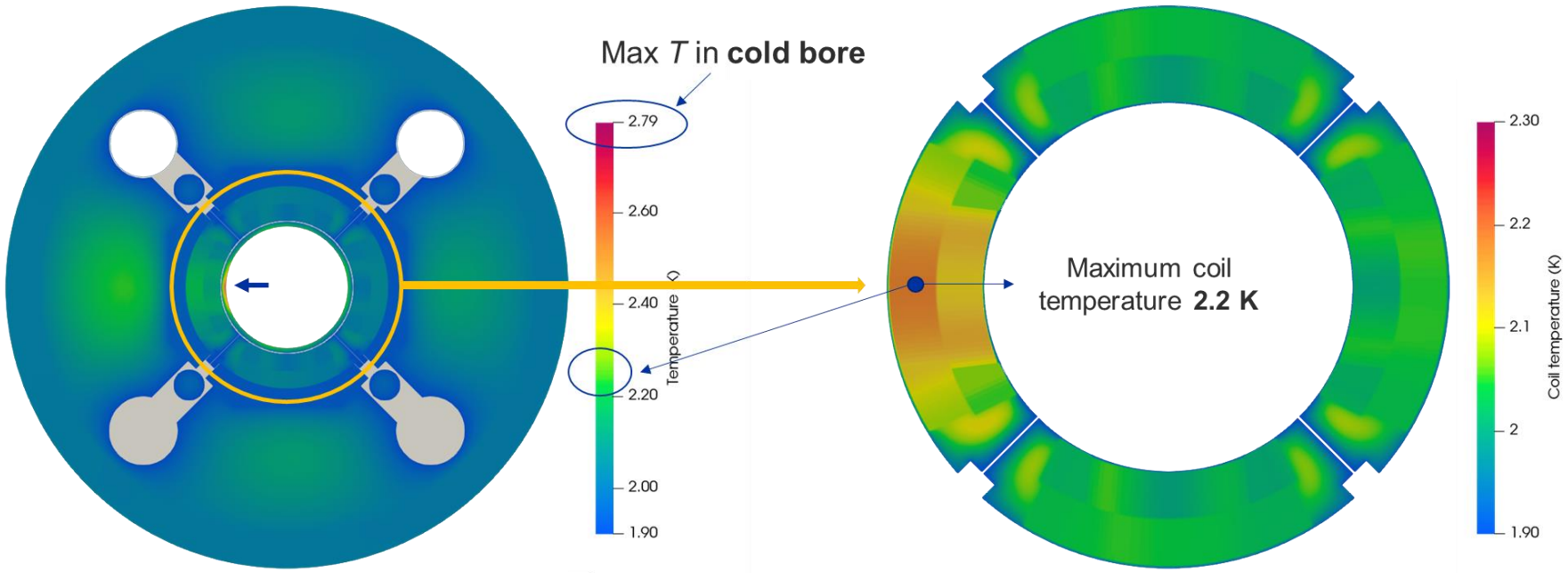

NB: Cold bore included, luminosity = 5.0×10^{34} $cm^{-2}s^{-1}$

Results: example Q2B IR1-HC @ nominal luminosity

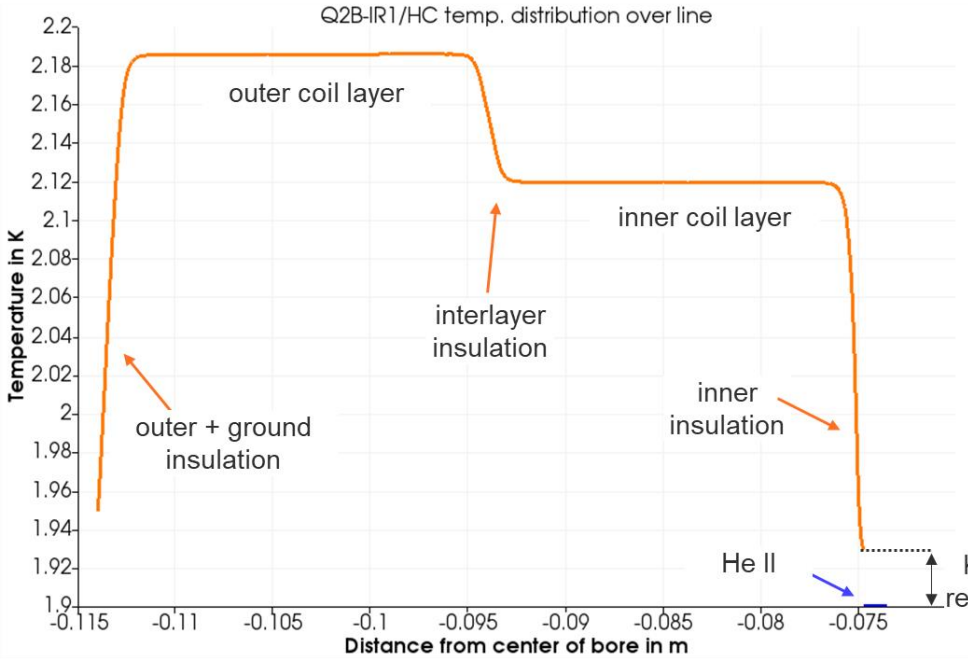

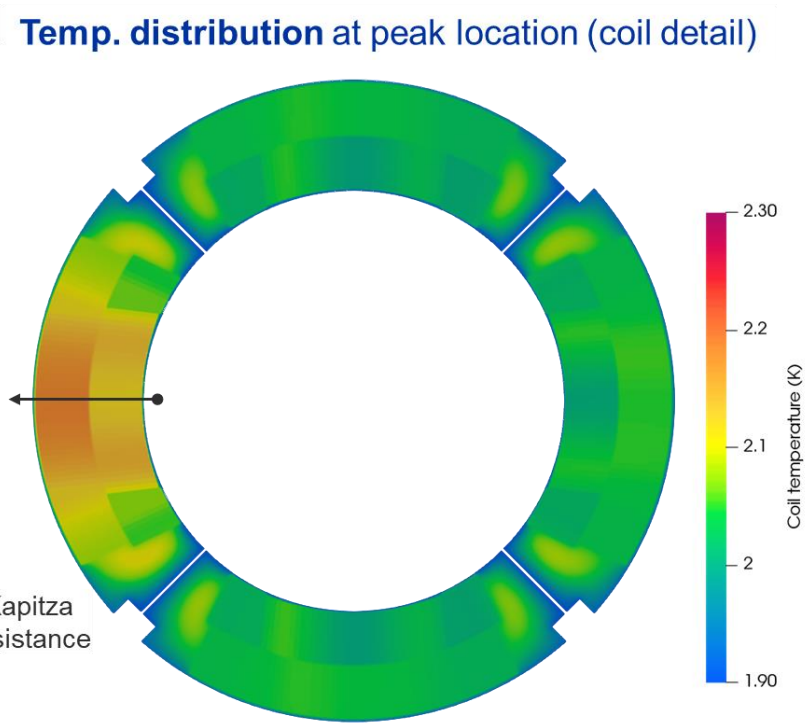

With fully impregnated cables, the thermal gradients are mainly determined by the interfaces (in contrast with NbTi-helium permeable cables)

With fully impregnated cables, the thermal gradients *are mainly determined by the interfaces* (in contrast with NbTi-helium permeable cables)

→ Going from fully helium-immersed coils to “dry” conduction-cooled coils is for fully impregnated cables, apart from an additional DT, a similar situation.

For future magnet development based on fully impregnated coils the temperature gradient ΔT across the coil must be kept as low as possible:

- Control the interfaces
  - Electrical insulation (Kapton foils p.e.)
  - Quench heaters (external, CLIQ, inductive…)
  - New impregnation materials (can we enhance the conductivity & Cp?)
- New conductors
  - Anisotropy of HTS tapes
  - Electrically insulated or non-insulated HTS tapes
  - …
- Conductivity & Cp data of new magnet designs to be measured
  - Accurate data greatly detailed thermal analysis

Key takeaways

- A **robust, easily adaptable numerical framework** has been consolidated to evaluate heat extraction mechanisms in **complex cryogenic system geometries involving He II**
- We are now able to produce results in a timeframe that allows for **parametric investigation of geometry, operational *T*, and power deposition** on magnet systems cooled by static, pressurised He II → this enables a **systematic approach**, and **can be used as a tool in magnet design** w.r.t. heat extraction
- Numerical simulations **directly benefit from the material data obtained from the experimental test campaign**, allowing for **more realistic, accurate calculations**
- The **heat extraction pathways for the HL-LHC inner triplet magnets have been validated** for the latest geometry, considering a steady-state power deposition at peak location for nominal operating conditions (5.0×10^{34} $cm^{-2}s^{-1}$, 7 TeV), at 1.9 K cold source

ASC 2022 paper submitted to *IEEE Transactions on Applied Superconductivity (TAS)*

Numerical Assessment of the Inhomogeneous Temperature Field and the Quality of Heat Extraction of Nb_3Sn Impregnated Magnets for the High Luminosity Upgrade of the LHC

Patricia Borges de Sousa, Kirtana Puthran, Marta Sabaté-Gilarte, Francesco Cerutti, Susana Izquierdo Bermudez, Ezio Todesco, Rob van Weelderen

Abstract—**The High Luminosity upgrade of the Large Hadron Collider (HL-LHC) at CERN foresees the installation of Nb3Sn-based quadrupole magnets at selected interaction points of the accelerator. The precise knowledge of each magnet's thermal characteristics and heat extraction performance in response to power depositions during both nominal and ultimate conditions is essential in determining safe operating margins. A 2D numerical framework has been developed to systematically assess the temperature distribution in the combined magnet structure-superfluid He system of each magnet and enveloping cold mass using open-source software. Here a full cross-section of a magnet cold mass is modelled, under the power density distribution expected at the most exposed longitudinal position during accelerator operation at an instantaneous luminosity of 5.0×10^{34} cm^{-2}s^{-1}, corresponding to the nominal conditions for HL-LHC. Temperature maps and margins are presented for the inner triplet magnets (MQXF) for both horizontal and vertical beam crossing conditions, along with the validation of the design of cold mass cooling channels for heat extraction.**

Index Terms— **cryogenics, numerical simulation/model, power deposition, Nb3Sn magnets, Helium II, HL-LHC**

I. Introduction

In the context of the High-Luminosity upgrade of the LHC at CERN, a robust multi-region CFD numerical toolkit using open-source software for the modeling of heat transfer in complex cryogenic system geometries involving He II has been developed, aiming to provide thermal design requirements [1] early enough in the design phase of the inner triplet magnets, such that they could be implemented in the mechanical design.

Previously established temperature margins along the full cross-section of inner triplet cold masses need to be updated to reflect changes in both power deposition by beam collision debris and coil layout, and to validate the heat extraction design that was originally proposed.

The work presented here in a continuation of previous studies [2]-[4], implementing updated MQXF geometry, power density maps and experimentally-obtained material properties, as well as a fully upgraded numerical toolkit that enables a systematic analysis of multiple magnet cross-sections and allows for parametric studies in a timely manner.

To model the temperature distribution in the combined solid–superfluid He system of each cold mass, the numerical toolkit itself and the 2D magnet model framework have been greatly refined. The model now includes seamless He II — He I phase-transitions and converges more than an order of magnitude faster.

II. Geometry and Numerical Toolkit

A. Geometry of MQXF cold mass

A 2D cross-section of a MQXF quadrupole magnet cold mass representative of the cold mass' straight section, along with the cold bore (see Fig. 1), was created according to the every 50 mm along the magnet axis and that connect the inner He annular space between the cold bore and the inner radius of the coil to the cooling channels, a continuous 1 mm slit along the titanium pole and G10 alignment key was created to enable a 2D geometry with equivalent longitudinal cross-section (see detail in Fig. 2 (a)).

Each component of the cold mass is assigned appropriate temperature-dependent material properties such as density, specific heat, and thermal conductivity. Whenever possible, material properties extracted from experimentally obtained data on MQXF coil samples [11] were used rather than literature values, the interface contact resistance between solid materials and He II was also experimentally measured on a MQXF coil sample.

B. Mesh creation and refinement

The geometry was meshed using a Python® API for the Meshing module of Salome® 9.7, with special refinement on the coil pack and thin layers such as insulation and helium passages. The final mesh used for the numerical calculations is composed of 3.5 million cells.

C. Numerical toolkit description

The numerical solver used in this work was implemented in OpenFOAM® v7, an open-source C++[5] toolbox for the development of customized solvers and libraries for solving continuum mechanics problems. A conjugate heat transfer solver was developed [12], combining a solver for heat conduction in composite solids and a solver for static He II (no flow").

Previously prohibitive computation time was drastically reduced by combining the calculation of the composite solid region (cold mass and cold bore) into a single region: as such, the complete geometry is composed of only two regions: a (composite) solid one, featuring many different zones each with its own material properties, and a pressurized He II region. The two regions interact by means of a baffle-type boundary condition that implements experimentally measured [11] interface contact resistance between He II and solid materials, referred to as Kapitza resistance.

III. Input for Simulation

A. Energy deposition from collision debris

Debris from proton-proton collisions at the interactions points induce energy deposition in the superconducting magnets and respective cold masses, especially those in the insertion regions (IR) [13]. The power density deposited in the coils leads to an increase in temperature that is non-uniform throughout the cold mass structure.

The temperature increase due to debris-generated energy deposition needs to be evaluated to provide a more realistic operating temperature field for the magnets in the insertion regions. The energy deposition in the inner triplet magnets in the insertion regions IR1 (ATLAS) and IR5 (CMS) used as input for the present work was estimated by FLUKA for a baseline He II heat exchangers is set at a fixed temperature of 1.9 K (see Fig. 2). Finally, the power density map obtained with FLUKA (for a luminosity of 5.0×10^{34} cm^{-2}s^{-1} and proton-proton collisions at a center-of-mass energy of 14 TeV) is applied to the entire cross-section of the MQXF coil and cold mass; this is the only input that varies with each of the 12 modeled magnet cross-sections.

IV. Results

A. Temperature maps

Results consist of a temperature map for each selected magnet cross-section: an example of power density (a) and resulting temperature profile (b) is shown in Fig. 3 for the most exposed cross-section of Q2B at insertion region 1 (horizontal crossing). There is a localized hotspot in the cold bore, reaching 2.5 K, where the power density is highest.

Fig. 4 (a) shows the same temperature profile as Fig. 3, focused only on the coil itself. The coil shows a fairly homogeneous temperature distribution, with a maximum calculated temperature of 2.22 K on the outer layer, *i.e.* a 0.32 K gradient with respect to the cooling source in the saturated He II heat

Fig. 4. (a) Example of magnet coil's temperature map resulting from the power deposition at peak location (shown Q2B in IR1, horizontal crossing, for nominal luminosity); the cold mass was omitted to highlight the coil. (b) Temperature profile along the horizontal cut shown in (a), highlighting the contributions of the different components to the established temperature gradient. Note the discontinuity between the He II bath at 1.9 K and the inner insulation due to Kapitza interface resistance.

and accurate temperature margin map. The minimum calculated temperature margin for each analyzed magnet cross-section is shown in Table I. The minimum value is invariably found in the cable(s) closest to the pole, where the magnetic flux density is highest. The rest of the coil has a calculated temperature margin above 5 K, considering an otherwise ideal conductor.

V. Conclusion

A robust, easily adaptable numerical toolkit has been consolidated to produce results in a timeframe that allows for parametric investigation of geometry, operational temperature, and power deposition on magnet systems cooled by stagnant, pressurized He II.

The heat extraction pathways that were defined in the design phase for the HL-LHC inner triplet magnets using earlier versions of the numerical framework have been reevaluated for the latest geometry, considering steady-state power deposition at peak location for nominal operating conditions (5.0×10^{34} cm^{-2}s^{-1}, 7 TeV), at a baseline cooling source temperature of 1.9 K.

For the cross-sections of each magnet at peak power density, a maximum temperature of 2.22 K was calculated on the coil pack (on Q2a, IR5), while the maximum temperature for the rest of the cold mass is invariably located on the cold bore, reaching 2.79 K on Q3b, IR5. These results compare positively against the conservative assessment made during the cold mass design phase [2].

Considering the calculated temperature distribution, for the design B_{op}-J_{op} and cold source at 1.9 K, on an otherwise ideal magnet, a minimum temperature margin of 4.78 K was found for a single conductor, nearest to the pole, in Q3a, IR5.

Acknowledgment

The authors would like to acknowledge the Cryolab team at CERN for their support in the experimental campaign on He II heat transfer to Nb3Sn magnet samples.

Helium availability and typical LHC reliance

(fully immersed magnets)

Next slides source: Frederic Ferrand (CERN Cryogenics)
see [7] for the full transcript

- Presentation based on available public information only
- Not an economist nor a seller, only interest is to supply necessary molecules for the laboratory in the coming years
- Helium market is currently (2022-data) evolving really fast and situation may be significantly different in a few months

Carte 1 : production, échanges et consommation d'hélium dans le monde en 2018

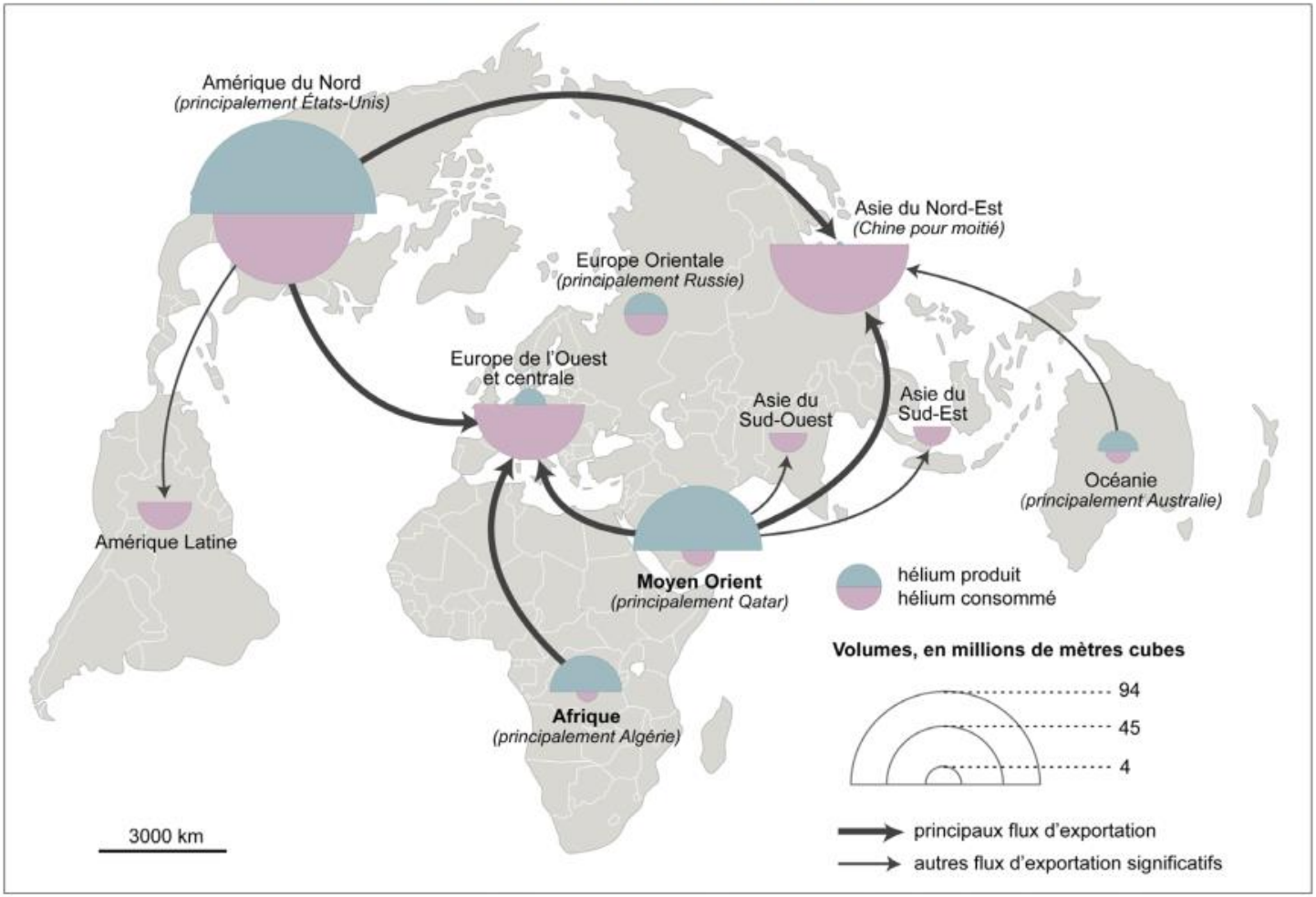

Source : Gubler et al. *(2019).*

Europe (and CERN) are outside supplier dependent

Ref: https://www.ifri.org/fr/publications/briefings-de-lifri/helium-nouvelles-geographies-dune-ressource-critique

Use of helium cryogenics at CERN

LHC & Experiments

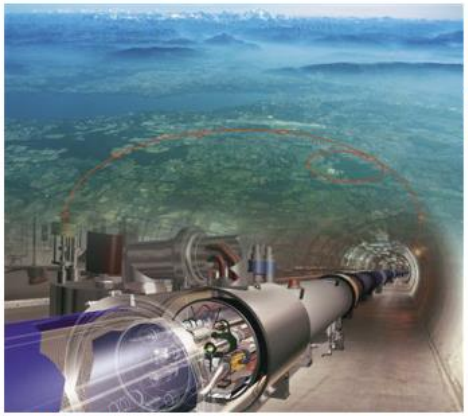

LHC 36'000 tonnes of cold mass distributed over the 26.7 km underground accelerator

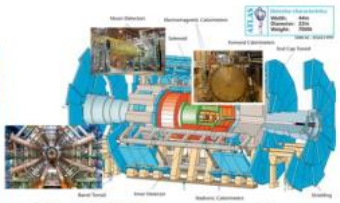

ATLAS 1'275 tonnes of cold mass

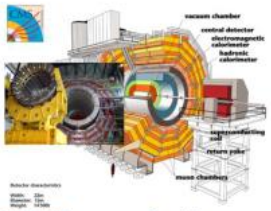

CMS 225 tonnes of cold mass

non-LHC & Test Facilities

SM18 test Facility

West Area test Facility

HIE Isolde Cryo Modules

SPS BA4 COLDEX

SPS BA6 Crab Cavities

Central Liquefier

North Area

LHC accelerator cooling of the superconducting magnets at 1.9 K
ATLAS cooling at 4.5 K of the superconducting magnetic system
CMS cooling at 4.5 K of the superconducting solenoid

Test Benches for accelerator magnets, wires, RF cavities
non-LHC facilities and **fixed target physics experiments**
Central Helium liquefier and **Cryogenics laboratory**

Courtesy Frederic Ferrand

LHC infrastructure

Surface storage & distribution

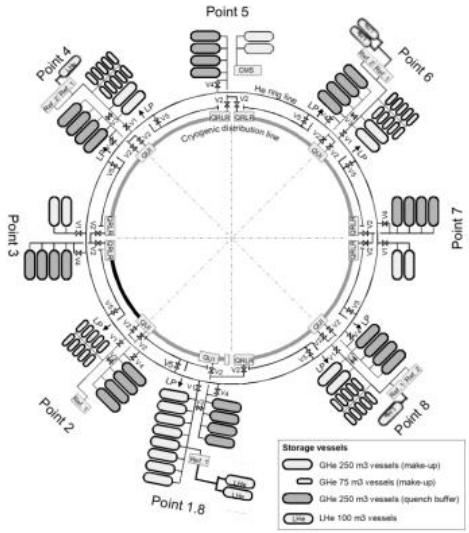

Gaseous helium storage 250m³

Liquid helium storage 250m³

Underground distribution & use

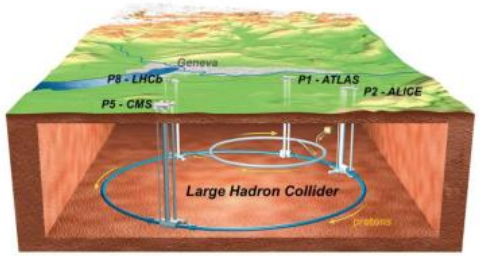

4.5K & 1.8K Cold Boxes

Distribution Valve Boxes

Distribution System

- Total inventory at CERN **175 tonnes** including **130 tonnes minimum for LHC**
- Distribution through the LHC Helium Ring Line, inter-sites High Pressure helium distribution line for non LHC and trailers

Courtesy Frederic Ferrand

Scope of supply for helium contracts 2022-2026

Liquid helium supply

200 tonnes

to compensate helium losses

Mainly for **testing and experiments**

For **LHC machine** constant effort to reduce losses showed results over the past 15 years

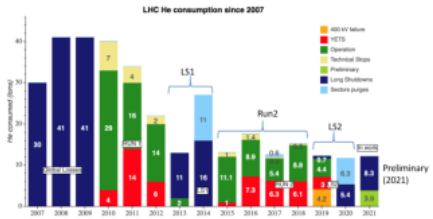

Helium quantities included:

- LHC needs for **Run 3** and refilling of the machine at the end of **Long Shutdown 3**
- Requirement for new **HL LHC cryogenic infrastructure** are also included

Helium management

140 tonnes

temporary sent out from CERN to contractual suppliers and returned on demand

This is a **necessary extension of CERN storage** capacity when LHC machine is partially or completely warm

During **Run year end closure up to 20 tonnes** are sent out for about 2 months

During **Long Shutdowns up to 80 tonnes** are sent out for about 18 months

Gaseous helium supply

6 tonnes

for LHC machine pressure tests

High Pressure helium trailers are used to pressurized sectors for safety pressure test

These deliveries are foreseen at the end of **Long Shutdown 3**

Courtesy Frederic Ferrand

Helium market long term evolution driven by US strategic decisions

Helium act 1925

- Significant increase of the production in the 60's
- Cliffside infrastructure and underground storage of the federal strategic reserve
- Almost monopoly of the US on the worldwide helium market
- Rapid decrease of production in the 70's, reaching peak in 1980
- Managed by the state BLM with significant associated costs
- Confort zone, low prospecting and investment elsewhere

Helium privatization act in 1996

- Federal government expenses pay back by selling 1bcm till 2015
- Large industrial investment in Algeria 1997 and Qatar since 2008
- Production capacity developments in the private sector was too low

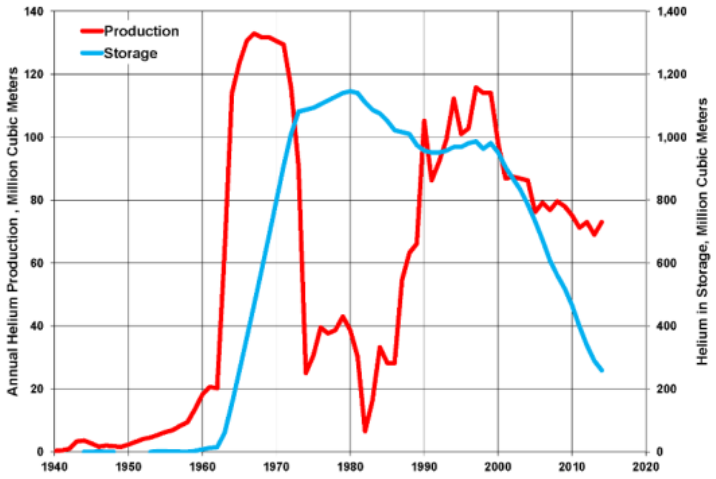

Wikipedia, based on US geological survey data

Stewardship Act of 2013

- Regulation of the of the market by selling of the strategic reserve through yearly auctions to the private sector
- Make the bridge with new international extraction capacity development
- Regulation of the US domestic market, but reduction of exports over the years

Good Read (in French): IFRI Briefing

Courtesy Frederic Ferrand

Known parameters affecting helium availability

- **Unbalanced supply and demand,** helium shortage 2006 & 2013
- **Geopolitical stability** in the country of extraction, Qatar 2017
- **Logistics complexity** blockage of Suez Canal in 2020
- **Maintenance shutdown or technical event** on LNG feed and helium liquefaction plants can impact market

Courtesy Frederic Ferrand

What's happening in 2022 ?

- **BLM closure** in January
  - Temporarily closed procedures for safe handling of chemical materials (Gasworld)
  - Outsource of BLM operations to private contractor
- **Explosion at AMUR** site in Russia production site in January
  - Several events leading to stop of the commissioning (Gasworld) ;
  - Expecting ramp up of the production postponed
- **Commercial limitation with Russia** due to conflict in Ukraine
  - Impact on the AMUR project repair and recommissioning of the helium plant
  - Takeover of the engineering from European by a Chinese company
- **Planned maintenance** during spring period
- **Restart of industrial activities** after Covid period

Courtesy Frederic Ferrand

Consequences

Current situation

- Market shortage is affecting industrial and scientific customers
- Manufacturing industry contracts are impacted with volume limitations
- Large scientific instrument cannot do so & rely on established industrial partnership

Helium market still at risk in 2023 and for the coming years

- Uncertainty on the effective Russian production capacity and market access
- Algerian gas production transferred using pipeline instead of LNG
- No more back-up from the US federal authorities, Cliffside for sale ! (C&en News)

Courtesy Frederic Ferrand

Perspective of new helium production capacities

- **LNG related**
  - Algeria debottlenecking of existing production sites
  - South Africa → 900Mm3 (lower estimate)
  - Qatar IV ?

- **Nitrogen-based helium production** (Physicsworld article)
  - Canada (Gasworld article 1 & article 2) → Announced production objectives 10% ww capacipty by 2030
  - Tanzania (The Citizen) 54bcf of primary helium at Lake Rukwa → Production announced in 2025

Courtesy Frederic Ferrand

Food for thought of operating fully helium immersed accelerator magnets

Disclaimer: the LHC has been an immense success and functions marvelously. A 27 km long accelerator of which about 23 km at 1.9 K!

A cryogenic success, on both magnet cooling as well as the whole cryogenic infrastructure which functions with very high availability!

However, there are a few points which are food for thought on whether we can do better for the next machine…
(whichever one that might be)

Safety: avoiding trapped volumes

What happens if one neglects (or even forgets) radial passages!

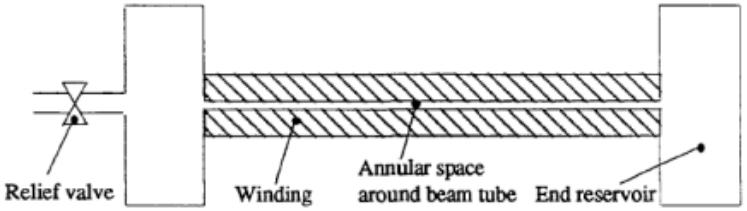

Figure 1.1 Dipole magnet

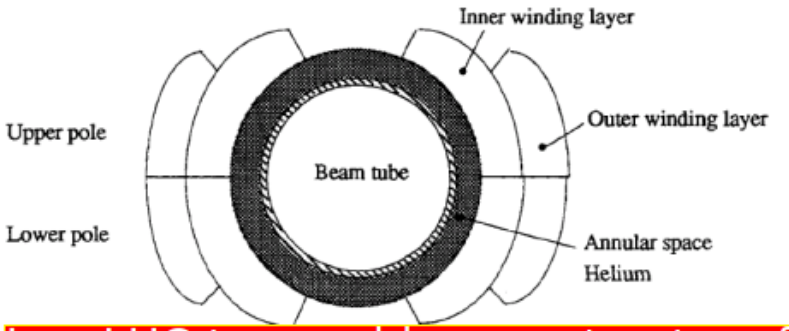

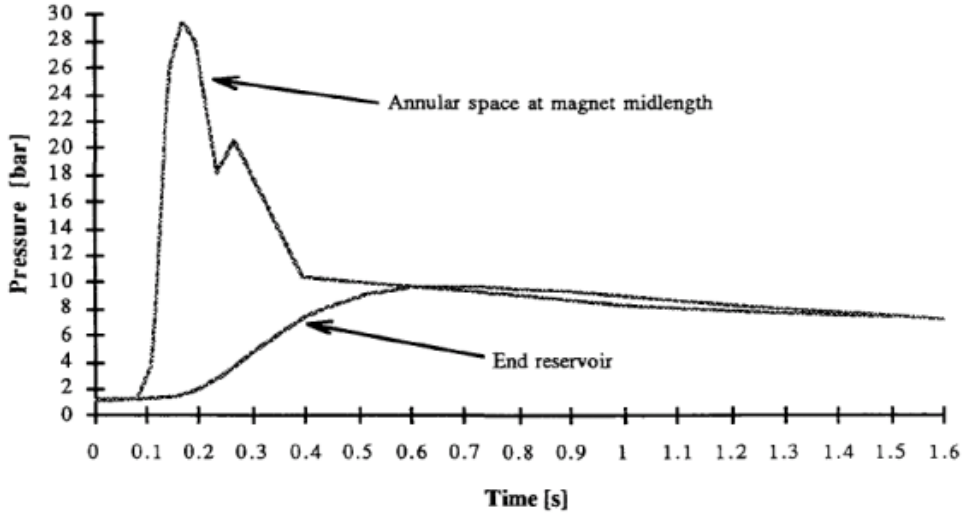

In a LHC-type cold-mass structure foreseen for a future 10 T coil, a low field (< 5 T) coil was placed, but to ease assembly a teflon sheet was mistakenly inserted between collar and yoke!

All radial escapes were closed, and even with the magnet energy of 5 T field, annular space pressures reached 30 bar.

A higher field coil of 10 T would have squeezed/distroyed the beam-pipe.

Safety: avoiding trapped volumes

- Since the experience with this very early stage LHC-cold mass test the explicit control of radial and longitudinal helium escape paths has become an integral part of the fully helium immersed magnet cold-mass designs and has never been an issue anymore

Safety: cold-mass pressure vessel

- A quench of a magnet-coil transfers about 25 % or more of the stored energy directly to the helium in which it is immersed
  - → pressure built up would be of the order of > 200 bar if not managed by safety relief devices
  - → The rate of pressure rise is coil-specific (porous or not p.e.) but initial adiabatic shock waves of several bar to about 10 bar cannot be avoided.
  - → The pressure rating of the cold-mass due to the helium pressure rise phenomena may be higher than desired because of this (think of machine-detector-interface magnets p.e.)

Safety: containing helium spill consequences

The shear amount of helium inside accelerator magnets has a heavy impact on personnel safety, especially in underground areas, and the infrastructure to deal with this:

- Helium release has to be captured in dedicated cryogenic transfer lines
- Access restrictions for machine maintenance become dependent on the amount of helium in the cold-masses and their powering status
- Should accidents break the cold-mass to insulation vacuum helium will instead of being captured by the cryogenic transfer line spill into the ambient environment → Asphyxiation hazard

Inventory handling and supplier dependence

Some points to remember

Energy efficiency: Incorporate in the magnet design, whenever possible, features to intercept heat at as high T as possible!

Energy efficiency: If possible, use conductors that have a high Tc

Facilitating robust thermal design: Incorporate temperature margin to deal with heat extraction (no magnet operates at an ideal homogeneous temperature)

Inventory handling, supplier dependence, general & personnel safety: Aim for reduced helium content, preferably conduction cooled magnets

Selected References (1/3)

Books

“Experimental Techniques for Low-Temperature Measurements - Cryostat Design, Material Properties, and Superconductor Critical-Current Testing”, *Jack W. Ekin, Oxford University Press 2006, ISBN 0–19–857054–6 978–0–19–857054–7*

“Cryostat Design - Case Studies, Principles and Engineering“, *J.G. Weisend II, SPRINGER 2016, ISSN 0538-7051 ISSN 2199-3084 (electronic) International Cryogenics Monograph Series ISBN 978-3-319-31148-7 ISBN 978-3-319-31150-0 (eBook) DOI 10.1007/978-3-319-31150-0*

“Helium Cryogenics”, *Steven W. Van Sciver, SPRINGER, ISBN 978-1-4419-9978-8 e-ISBN 978-1-4419-9979-5 DOI 10.1007/978-1-4419-9979-5*

References (2/3)

[1] COOLING STRINGS OF SUPERCONDUCTING DEVICES BELOW 2 K: THE HELIUM II BAYONET HEAT EXCHANGER, *Ph. Lebrun, L. Serio, L. Tavian and R. van Weelderen, LHC-project-report-144 / CEC-ICMC'97 - Portland - OR - USA July 28th - August 1st 1997*

[2] SUPERFLUID HELIUM AS A TECHNICAL COOLANT, *Ph. Lebrun, LHC Project Report 125, Presented at 15th UIT National Heat Transfer Conference - Torino - Italy, June 19-20 1997*

[3] Deduction of Steady-State Cable Quench Limits for Various Electrical Insulation Schemes with Application to LHC and HL-LHC Magnets, *Pier Paolo Granieri, Rob van Weelderen, CERN-ACC-2014-0035, 20/02/2014*

[4] *Development and application of a generic CFD toolkit covering the heat flows in combined solid-liquid systems with emphasis on the thermal design of HiLumi superconducting magnets*, Gennaro Bozza, Ziemowit M. Malecha, Rob Van Weelderen, Cryogenics-D-15-00175 (CHATS-2015 workshop)

References (3/3)

[5] An experimental and numerical framework to assess the temperature distribution in complex He II-cooled magnet geometries, *Kirtana Puthran, Patricia Borges de Sousa, Lise Murberga, Torsten Koettig, Rob van Weelderen, CHATS-AS 2023 Torino (to be published)*

[6] Numerical assessment of the inhomogeneous temperature field and the quality of heat extraction from Nb_3Sn impregnated magnets for the High Luminosity upgrade of the LHC, *Patricia Borges de Sousa, Kirtana Puthran, Marta Sabaté-Gilarte, Francesco Cerutti, Susana Izquierdo Bermudez, Ezio Todesco, and Rob van Weelderen, ASC 2022 – Honolulu, (to be published)*

[7] “Helium market considerations - Muon Magnets Working Group”, *Frederic Ferrand (CERN Cryogenics), https://indico.cern.ch/event/1183565/*